

Magnification effect on the detection of primordial non-Gaussianity from photometric surveys

Toshiya Namikawa*

*Department of Physics, Graduate School of Science,
The University of Tokyo, Tokyo 113-0033, Japan*

Tomohiro Okamura†

Astronomical Institute, Tohoku University, Sendai 980-8578, Japan

Atsushi Taruya‡

*Research Center for the Early Universe, School of Science,
The University of Tokyo, Bunkyo-ku, Tokyo 113-0033, Japan and
Institute for the Physics and Mathematics of the Universe,
The University of Tokyo, Kashiwa, Chiba 277-8568, Japan*

(Dated: February, 2011)

We present forecast results for constraining the primordial non-Gaussianity from photometric surveys through a large-scale enhancement of the galaxy clustering amplitude. In photometric surveys, the distribution of observed galaxies at high redshifts suffers from the gravitational-lensing magnification, which systematically alters the number density for magnitude-limited galaxy samples. We estimate size of the systematic bias in the best-fit cosmological parameters caused by the magnification effect, particularly focusing on the primordial non-Gaussianity. For upcoming deep and/or wide photometric surveys like HSC, DES and LSST, the best-fit value of the non-Gaussian parameter, f_{NL} , obtained from the galaxy count data is highly biased, and the true values of f_{NL} would typically go outside the $3\text{-}\sigma$ error of the biased confidence region, if we ignore the magnification effect in the theoretical template of angular power spectrum. The additional information from cosmic shear data helps not only to improve the constraint, but also to reduce the systematic bias. As a result, the size of systematic bias on f_{NL} would become small enough compared to the expected $1\text{-}\sigma$ error for HSC and DES, but it would be still serious for deep surveys with $z_{\text{m}} \gtrsim 1.5$, like LSST. Tomographic technique improves the constraint on f_{NL} by a factor of 2-3 compared to the one without tomography, but the systematic bias would increase.

I. INTRODUCTION

Any hints on primordial non-Gaussianity would be fruitful to clarify the generation mechanism for primordial density fluctuations in the early stage of the Universe. Since the single-field slow-roll inflationary scenario predicts nearly Gaussian fluctuations (e.g., [1–7]), a detection of large primordial non-Gaussianity will rule out the simplest inflationary model and provides us a new insight into the physics in the early universe.

Traditional and popular method to detect primordial non-Gaussianity is to measure the three-point correlations of statistical fields (e.g., [8–13]). This correlation vanishes in the Gaussian fields, and non-vanishing signals of the three-point correlations would provide information on primordial non-Gaussianity.

On the other hand, recent numerical and theoretical studies (e.g., [11, 14–25]) have revealed that the local-type non-Gaussianity, originating from the non-linear dynamics of scalar fields on super horizon scales, can induce a large-scale enhancement in the galaxy clustering am-

plitude. In the local-type non-Gaussianity, the primordial fluctuations characterized by the Bardeen potential, $\Phi(\mathbf{x})$, are described by the Taylor expansion of Gaussian field $\phi(\mathbf{x})$ as (e.g., [4, 8, 26, 27]):

$$\Phi(\mathbf{x}) = \phi(\mathbf{x}) + f_{\text{NL}}(\phi^2(\mathbf{x}) - \langle \phi^2 \rangle). \quad (1)$$

The non-vanishing parameter, $f_{\text{NL}} \neq 0$, implies a departure from the Gaussian statistics, and even a small value of f_{NL} has been found to produce a scale-dependent galaxy bias, which is prominent on large scales and at high redshifts. With a help of this property, the constraint on primordial non-Gaussianity has been obtained recently, combining photometric and spectroscopic surveys [28–30], and it turned out that the results are rather comparable to that from CMB observation. This constraint mainly comes from the quasar data obtained from photometric surveys, which are wider and deeper than spectroscopic surveys with a limited observation time. In this respect, wide and deep photometric surveys planned to start in the near future such as Subaru Hyper Suprime-Cam (HSC) survey [31], Dark Energy Survey (DES) [32], and Large Synoptic Survey Telescope (LSST) survey [33]) would provide a more stringent constraint on primordial non-Gaussianity.

In those photometric surveys, the observed galaxy distribution at high redshifts often suffers from the magni-

* namikawa@utap.phys.s.u-tokyo.ac.jp

† t-okamura@astr.tohoku.ac.jp

‡ ataruya@utap.phys.s.u-tokyo.ac.jp

fication effect due to the gravitational lensing, which apparently changes the number density of observed galaxies [34–36]. As increasing redshift, since the amplitude of the density fluctuations becomes small and the observed angular separation between any pairs of two sources decreases, the galaxy auto-angular power spectrum is shifted to small scales with the amplitude decrease. On the other hand, the lensing contribution on the angular correlations become significant at higher redshifts. As a result, the contribution of the magnification effect on the galaxy auto correlations is expected to be significant not only at high redshifts, but also on large angular scales. We thus naively expect that the magnification effect can mimic the scale-dependent galaxy bias, and ignoring magnification effect in the theoretical template for angular correlations would lead to a biased estimation of primordial non-Gaussianity.

In this paper, we study the potential impacts of the magnification effect on constraining primordial non-Gaussianity from the upcoming photometric surveys. There are several studies forecasting constraints on primordial non-Gaussianity through the scale-dependent galaxy bias (e.g., [29, 37–39]). Here, we pay a particular attention to the magnification effect, and quantitatively evaluate the systematic biases arising from the incorrect treatment of the magnification effect in estimating the non-Gaussianity parameter f_{NL} , which has never been considered in the previous forecast studies. Further, we discuss the role of the cross correlation statistics between galaxy number density and other observables such as cosmic shear. This has been also never investigated in previous works, since the cross correlation signals are basically insensitive to the primordial non-Gaussianity compared to the galaxy auto correlations. However, we found that the cosmic shear-galaxy count cross-correlations have large signal-to-noise ratios, and help not only to improve the constraint on f_{NL} , but also to reduce the systematic bias.

This paper is organized as follows. In Sec.II, we briefly review the scale-dependent galaxy bias induced by the primordial non-Gaussianity, and describe how the magnification effect changes the number density of observed galaxies. We then give the formalism for the angular power spectra obtained from photometric galaxy surveys. In Sec.III, we explicitly compute the angular power spectra and calculate the signal-to-noise ratios for auto and cross power spectra of galaxy count and cosmic shear. In Sec.IV, based on the Fisher matrix formalism, we quantitatively estimate the impact of magnification effect on the detection of primordial non-Gaussianity, particularly focusing on three representative surveys, i.e., HSC, DES and LSST. Finally, Sec.V is devoted to the summary and discussion.

Throughout the paper, all the angular power spectra are computed from the modified version of cosmological Boltzmann code, CAMB [40], with the following set of cosmological parameters assuming a flat Lambda-CDM model, which is consistent with WMAP7 results [41];

$\Omega_b h^2 = 0.022$, $\Omega_m h^2 = 0.13$, $\Omega_\Lambda = 0.72$, $n_s = 0.96$, $A_s = 2.4 \times 10^{-9}$, $\tau = 0.086$, and $w = -1$, for the density parameters of baryon and matter, dark energy density, scalar spectral index, scalar amplitude at $k = 0.002 \text{ Mpc}^{-1}$, reionization optical depth, dark-energy equation-of-state parameter, respectively. Unless otherwise stated, non-Gaussian parameter is set to $f_{\text{NL}} = 0$. The non-linear power spectrum is computed according to the fitting formula given in Ref.[42].

II. PROBING PRIMORDIAL NON-GAUSSIANITY FROM PHOTOMETRIC SURVEYS

A. Primordial non-Gaussianity imprinted on galaxy bias

In the presence of local-type primordial non-Gaussianity, recent numerical and theoretical studies on the clustering of halos/galaxies (e.g., [14–23]) show that there appears a scale-dependent enhancement of the clustering amplitude on very large scales. Theoretically, the scale-dependent property of the halo/galaxy bias can be explained by a tight correlation between long-wavelength and short-wavelength modes, which usually vanishes in the Gaussian case. Especially, the modulation of short-wavelength modes responsible for forming halos is induced by the Newton potential or Bardeen potential $\Phi(\mathbf{x})$. This fact leads to a strong scale-dependence for the fluctuations of halo/galaxy number density on large scales, and in Fourier space, we obtain [28, 43]

$$g(\mathbf{k}, z) = [b_G + \Delta b(k, z)]\delta(\mathbf{k}, z), \quad (2)$$

where $g(\mathbf{k}, z)$ and $\delta(\mathbf{k}, z)$ are the fluctuations of galaxy number density and matter density fluctuations, respectively, and the quantity b_G implies the galaxy bias in the case of Gaussian initial condition. The function $\Delta b(k, z)$ represents the non-Gaussian correction, which is given by [28, 43]

$$\Delta b(k, z) = f_{\text{NL}} A_{\text{NG}} \frac{3\Omega_m H_0^2}{k^2 \mathcal{T}(k) D(z)}. \quad (3)$$

Here, the quantity Ω_m is the matter energy density, H_0 denotes the Hubble parameter at present, $D(z)$ is the linear growth rate, and $\mathcal{T}(k)$ is the transfer function for linear matter density fluctuations, which is set to unity in the limit $k \rightarrow 0$. Thus, in the large-scale limit ($k \rightarrow 0$), the second term in Eq.(2) becomes dominant, and the enhancement of clustering amplitude is prominent in a scale-dependent way. Since this term is inversely proportional to the growth rate $D(z)$, non-Gaussian correction becomes also significant at higher redshifts.

Assuming the universality of mass function, the quantity, A_{NG} , gives $\delta_c(b_G - 1)$ [14, 28], and the quantity $\delta_c = 1.68$ is the critical density for a spherical collapse. As advocated by several papers, however, the quantity

A_{NG} would not be simply related to the halo mass function, but depends on the merger history of halo/galaxy samples [43]. In other words, we may have to determine A_{NG} from the observational data in practice. If this is the case, the non-Gaussian parameter f_{NL} would be completely degenerated with the quantity A_{NG} , and we need additional information on f_{NL} like the galaxy bispectrum in order to break the degeneracy. Our primary focus here is to explore the impact of magnification effect on the non-Gaussian parameter, and we simply assume $A_{\text{NL}} = \delta_c(b_G - 1)$ in the subsequent analysis. The influence of the magnification effect is a generic issue to constrain f_{NL} from the photometric surveys, and we expect that the results in the paper are also applicable to the case to combine other observations in breaking the degeneracy with A_{NG} .

B. Magnification effect on galaxy number density

The number density of galaxies obtained from photometric surveys often suffers from the magnification effect by the weak gravitational lensing of the large-scale structure (e.g., [44–46]). Since the gravitational lensing changes the apparent magnitude and the area of the patch in the observed sky, it also changes the observed galaxy number density. Denoting the zero-mean fluctuations of the observed galaxy number density along a direction $\hat{\theta}$ at redshift z by $n(\hat{\theta}, z)$, we have [46]

$$n(\hat{\theta}, z) = g(\hat{\theta}, z) + (5s(z) - 2)\kappa(\hat{\theta}, z), \quad (4)$$

where the quantity $\kappa(\hat{\theta}, z)$ is the lensing convergence at the position of source galaxy, and characterizes the change of the size of images. The convergence is given by [46]

$$\kappa(\hat{\theta}, z) = \frac{3\Omega_m H_0^2}{2} \int_0^{\chi(z)} d\chi \frac{\chi(\chi(z) - \chi)}{\chi(z)} \delta(\chi\hat{\theta}, \chi), \quad (5)$$

with the function $\chi(z)$ being the comoving distance. The second $(5s(z)\kappa)$ and third term (-2κ) in Eq. (4) arise from the modification of apparent magnitude and the area of the patch in the observed sky by lensing, respectively.

The magnitude of the lensing effect depends on the slope parameter, $s(z)$. Denoting the number of galaxies at redshift z , brighter than the magnitude m by $N(z, < m)$, the quantity $s(z)$ is defined by [46]

$$s(z) \equiv \frac{d \log_{10} N(z, < m)}{dm}. \quad (6)$$

Note that in addition to the correction in Eq. (4), there exists another possible contribution related to the lensing effect, which has been addressed in Refs. [47, 48]. That is, the observed galaxies are selected according not only to the magnitude cut, but also to the size cut, and the latter also alters the galaxy number density. Nevertheless, the

effect of size cut is basically proportional to the lensing convergence, and can be incorporated into the expression (4), with a slight change of the meaning of slope index, $s(z)$. In this respect, the results in the present paper is general, and applicable to the case taking account of the size cut.

C. The angular power spectra

The angular power spectra are the fundamental statistical quantity obtained from the photometric survey, and have a rich cosmological information. Here we write down the expressions for angular power spectra of galaxy number counts and cosmic shear obtained from photometric surveys.

The galaxy number density observed via photometric survey is projected onto the two-dimensional sky, and redshift information is obtained by dividing photometric galaxy samples into several subsamples binned with redshifts. With the redshift distribution of galaxies in i -th bin, $N_i(z)$, the two-dimensional distribution of observed galaxies in i -th bin, $n_i(\hat{\theta})$, are given by

$$n_i(\hat{\theta}) = \int dz \frac{N_i(z)}{\bar{N}_i} n(\hat{\theta}, z). \quad (7)$$

The quantity \bar{N}_i is the average number density per square arcminute in i -th bin, defined by

$$\bar{N}_i = \int_0^\infty dz_s N_i(z_s). \quad (8)$$

On the other hand, the cosmic shear is measured from the ellipticity of each galaxy image. Using the photometric redshift information, we can also divide the estimated shear into several redshift bins. We denote the cosmic shear field in the i -th redshift bin by $\gamma_i(\hat{\theta})$. Then, the angular power spectra between the observables, X and Y (X and Y are either of γ_i or n_j) are given by the following expression:

$$C_\ell^{XY} = \frac{2}{\pi} \int \frac{dk}{k^2} P_{\text{init}}(k) \Delta_\ell^X(k) \Delta_\ell^Y(k), \quad (9)$$

where $P_{\text{init}}(k)$ is the matter power spectrum at an early time and k is the Fourier wave number. The functions $\Delta_\ell^X(k)$ and $\Delta_\ell^Y(k)$ are one of the following [49–51]:

$$\Delta_\ell^{\gamma_i}(k) = \sqrt{\frac{(\ell+2)!}{(\ell-2)!}} \mathcal{P}_\ell(k; N_i(z)), \quad (10)$$

$$\Delta_\ell^{n_i}(k) = k^2 \int dz [b_G + \Delta b(k, z)] \frac{N_i(z)}{\bar{N}_i} D(z) j_\ell(k\chi(z)) + (5s_i - 2)\ell(\ell+1) \mathcal{P}_\ell(k; N_i(z)). \quad (11)$$

The function j_ℓ is the spherical Bessel function and

$\mathcal{P}_\ell(k; N_i(z))$ is defined by

$$\begin{aligned} \mathcal{P}_\ell(k; N_i(z)) &= \frac{3\Omega_m H_0^2}{2} \int_0^\infty dz_s \frac{N_i(z_s)}{\bar{N}_i} \\ &\times \int_0^{\chi(z_s)} d\chi \frac{\chi(z_s) - \chi}{\chi(z_s)\chi} \frac{D(z(\chi))}{a(\chi)} j_\ell(k\chi). \end{aligned} \quad (12)$$

The quantity s_i is the slope index in the i -th redshift bin. Although the slope index seems to have a strong redshift dependence [50, 52], we here assume the constant slope index within each redshift bin, and study the effect of time varying slope index.

Note that for the photometric redshift determination, the uncertainty arising from the photometric redshift error is crucial for the cosmological analysis [53]. To mimic this effect, we suppose that the photometric redshift estimates are distributed as a Gaussian with rms fluctuation $\sigma(z)$. Then the actual redshift distribution for i -th galaxy subsamples over the range, $z_{i-1} < z < z_i$, is related to the redshift distribution of galaxies, $N(z)$, as [54]

$$N_i(z) = \frac{1}{2} N(z) \left[\operatorname{erfc} \left(\frac{z_{i-1} - z}{\sqrt{2}\sigma(z)} \right) - \operatorname{erfc} \left(\frac{z_i - z}{\sqrt{2}\sigma(z)} \right) \right], \quad (13)$$

where the function $\operatorname{erfc}(x)$ is the complementary error function defined by

$$\operatorname{erfc}(x) \equiv \frac{2}{\sqrt{\pi}} \int_x^\infty dz \exp(-z^2). \quad (14)$$

III. MAGNIFICATION EFFECT ON ANGULAR POWER SPECTRA AND SIGNAL-TO-NOISE RATIO

In this section, adopting a simple model of time evolution for bias parameter b_G , we compute the angular power spectra, and show how the magnification effect changes the amplitude of angular power spectra. Also, based on the fiducial setup of future photometric surveys, we estimate the signal-to-noise ratios for auto- and cross-power spectra of galaxy counts and cosmic shear.

In Eq. (2), while the parameter b_G is assumed to be scale-independent on large-scales, it would manifest a strong time dependence. We characterize this by introducing the following function (e.g., [55–57]):

$$b_G = b_0 + \frac{b_z}{D(z)}. \quad (15)$$

Here, we set $b_0 = 1.5$ and $b_z = 2.0$ for fiducial values of the galaxy bias parameters. Since the photometric redshift information is available for most of the photometric surveys, we employ the tomographic technique, and divide all the galaxy samples into the three redshift subsamples. The redshift ranges for each bin are chosen as, $z < 0.739$, $0.739 < z < 1.14$, and $1.14 < z$, so that each redshift bin has the same number of galaxies. We

assume the redshift distribution of galaxies $N(z)$ as (e.g., [58])

$$N(z) = N_g \frac{3z^2}{2(0.64z_m)^3} \exp \left[- \left(\frac{z}{0.64z_m} \right)^{3/2} \right], \quad (16)$$

where the quantities N_g and z_m are the total number of galaxies per square arcminute and mean redshift. As typical values of the upcoming deep surveys, we set N_g to 35 arcmin⁻² and $z_m = 1.0$. As for the photo- z error, we adopt the simple scaling relation [54]:

$$\sigma(z) = 0.03 (1 + z). \quad (17)$$

Finally, the influence of magnification effect on the angular power spectra depends on the slope parameter, for which we set $s_1 = 0.5$, $s_2 = 1.0$, and $s_3 = 1.5$, close to the recently estimated values from the observations [50, 52].

A. Magnification effect on angular power spectra

In the presence of the magnification effect, the galaxy auto-power spectra, $C_\ell^{n_i n_j}$, and the shear-galaxy cross-power spectra, $C_\ell^{\gamma n_i}$, can be separately decomposed into several pieces:

$$C_\ell^{n_i n_j} = C_\ell^{g_i g_j} + C_\ell^{g_i \mu_j} + C_\ell^{\mu_i g_j} + C_\ell^{\mu_i \mu_j}, \quad (18)$$

$$C_\ell^{\gamma n_j} = C_\ell^{\gamma_i g_j} + C_\ell^{\gamma_i \mu_j}, \quad (19)$$

where the subscripts g_i and μ_i respectively represent the contribution of the *pure* galaxy clustering and magnification, which are identified with the first and second terms in Eq. (11). That is, the power spectra involving g_i and μ_i can be computed by simply neglecting the second and first terms in Eq. (11), respectively.

In Fig. 1, the galaxy auto and shear-galaxy cross angular power spectra ($C_\ell^{n_3 n_3}$ and $C_\ell^{\gamma n_3}$) are shown. We plot the power spectra in the presence/absence of the magnification effect for the Gaussian initial condition (black solid/red dotted), and also show the power spectra in the absence of the magnification effect for the non-Gaussian case, $f_{NL} = \pm 10$ (magenta solid). Note that the power spectra plotted here are independent of N_g in Eq. (16) (see Eqs. (10)-(12)).

For the galaxy auto power spectra $C_\ell^{n_3 n_3}$, there appears two contributions of the magnification effect in Eq. (18), i.e., $C_\ell^{\mu_3 \mu_3}$ and $C_\ell^{g_3 \mu_3}$. As shown in the top panel of Fig. 1, the cross power spectrum between galaxy counts and the magnification, $C_\ell^{g_3 \mu_3}$ (green dot-dashed), has similar angular dependence to $C_\ell^{g_3 g_3}$ (red dotted), and it slightly changes the overall amplitude of power spectra. The contribution of magnification auto-power spectra, $C_\ell^{\mu_3 \mu_3}$ (blue dotted), has also similar ℓ -dependence, but the amplitude exceeds $C_\ell^{g_3 \mu_3}$ on large scales. This feature comes from the fact that the weak lensing effect is mainly attributed to the growth of structure at lower redshifts. In the same manner, in the bot-

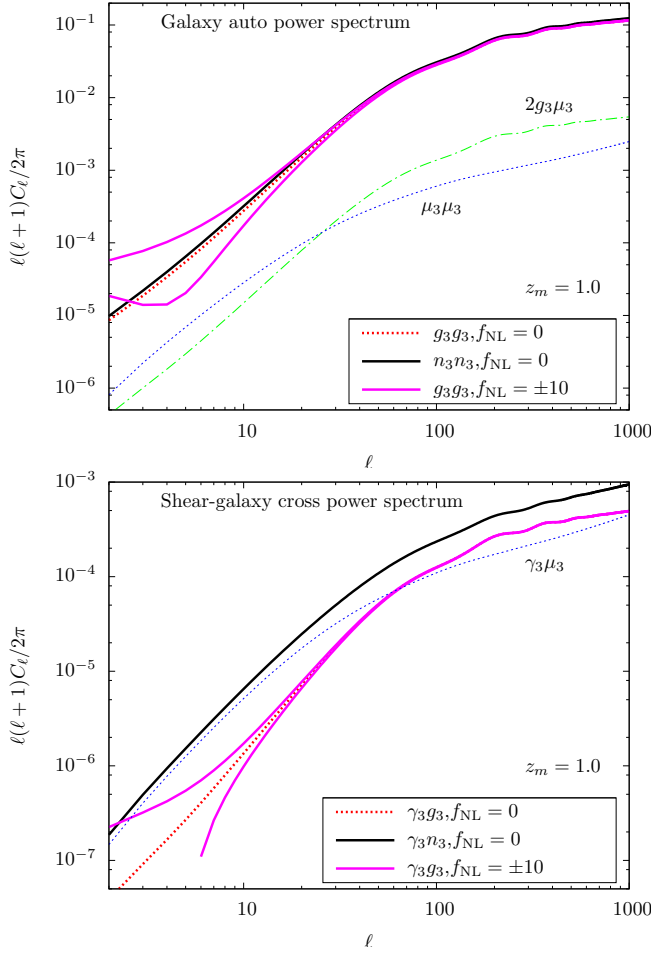


FIG. 1. The galaxy auto-power spectrum C_ℓ^{nn} (top) and the shear-galaxy cross-power spectrum $C_\ell^{\gamma n}$ (bottom). We plot the angular power spectra in the presence/absence of the magnification effect (black solid/red dotted) for the Gaussian initial condition, $f_{NL} = 0$, and also show the angular power spectra in the absence of the magnification effect in the non-Gaussian case, $f_{NL} = \pm 10$ (magenta solid). For comparison, we plot the contribution of the magnification effect ($2g_3\mu_3$, and $\mu_3\mu_3$ in the top and $\gamma_3\mu_3$ in the bottom panel).

tom panel of Fig. 1, the amplitude of shear-galaxy cross-power spectra, $C_\ell^{\gamma g_3}$, is enhanced at low- ℓ by the magnification effect. Hence, the magnification effect leads to a scale-dependent enhancement in the amplitude of angular power spectra, which can mimic the effect of primordial non-Gaussianity through the scale-dependent galaxy bias. On the other hand, the bias parameters b_0 and b_z are independent of the scales, and their influences appear not only on large scales but also on small scales. Thus, even if treating these as free parameters and marginalizing over them, the constraint on f_{NL} seems to be unaffected by the galaxy bias parameters b_0 and b_z .

In Fig. 2, to elucidate the scale-dependent enhancement of the power spectra on large scales, we plot the fractional difference of the galaxy auto power spectra,

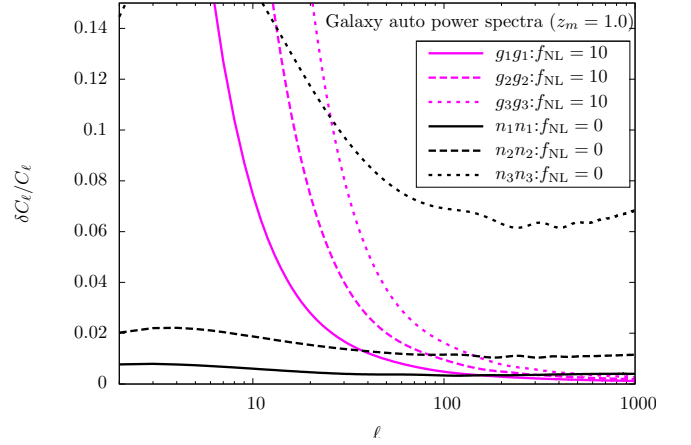


FIG. 2. The dependence of galaxy auto-power spectra on the parameter f_{NL} and the magnification effect for each tomographic bin. We define the fractional difference of galaxy auto-power spectra, $\delta C_\ell/C_\ell$ which is given in two cases: $C_\ell^{g_i g_i}(f_{NL} = 10)/C_\ell^{g_i g_i}(f_{NL} = 0) - 1$ (magenta lines) and $C_\ell^{n_i n_i}(f_{NL} = 0)/C_\ell^{g_i g_i}(f_{NL} = 0) - 1$ (black lines). The solid, dashed and dotted lines represent $(i, j) = (1, 1)$, $(2, 2)$ and $(3, 3)$ bin, respectively.

$\delta C_\ell/C_\ell$. Here, we examine the two cases: $C_\ell^{g_i g_i}(f_{NL} = 10)/C_\ell^{g_i g_i}(f_{NL} = 0) - 1$ (magenta lines) and $C_\ell^{n_i n_i}(f_{NL} = 0)/C_\ell^{g_i g_i}(f_{NL} = 0) - 1$ (black lines). As we expected, the impact of magnification effect is significant at higher redshift bins. This is because, as increasing the source redshifts, the gravitational lensing becomes significant and the amplitude of fluctuations g conversely decreases. The contribution of primordial non-Gaussianity is also significant at higher redshifts, because the non-Gaussian correction in the scale-dependent galaxy bias is proportional to the inverse of growth function, $D(z)$ [see Eq.(3)]. Note, however, that the redshift dependence of the magnification effect (magenta lines) is rather different from that of the scale-dependent galaxy bias (black lines). This implies that the tomographic technique is useful to break the degeneracy between the effects of magnification and primordial non-Gaussianity.

B. Signal-to-noise ratio

Since the magnification effect enhances the amplitude of power spectra especially on large scales, the signal-to-noise ratio for angular power spectra would be changed. To estimate the size of this, in Fig. 3, we plot the signal-to-noise ratios for galaxy auto and shear-galaxy cross spectra in the presence or absence of the magnification effect. The signal-to-noise ratio, S/N, is defined by

$$\frac{S}{N} \equiv \sqrt{\sum_{\ell=2}^{\ell_{\max}} \left(\frac{C_\ell^{XY}}{\Delta C_\ell^{XY}} \right)^2}, \quad (20)$$

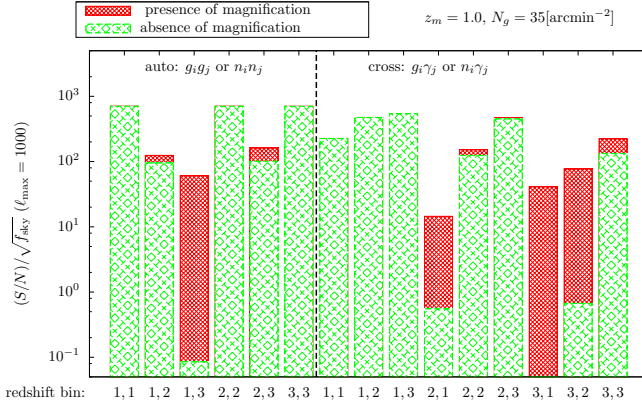


FIG. 3. The signal to noise ratio of each power spectra in the presence/absence of the magnification effect (red/green) for a survey with the mean redshift $z_m = 1.0$ and the number density of galaxy $N_g = 35 \text{ arcmin}^{-2}$. We show the signal-to-noise ratio for all power spectra normalized by $\sqrt{f_{\text{sky}}}$ since the signal-to-noise ratio is proportional to $\sqrt{f_{\text{sky}}}$.

where the quantity ΔC_ℓ^{XY} is the statistical error for each power spectra, given by

$$(\Delta C_\ell^{XY})^2 = \frac{1}{(2\ell+1)f_{\text{sky}}} \left[(C_\ell^{XY} + N_\ell^{XY})^2 + (C_\ell^{XX} + N_\ell^{XX})(C_\ell^{YY} + N_\ell^{YY}) \right]. \quad (21)$$

Here, the parameter f_{sky} is the sky coverage of photometric survey, and N_ℓ^{XY} are the noise power spectra, which will be later given in Sec.IV [see Eqs. (24)-(26)]. In Fig. 3, the signal-to-noise ratios are computed with $\ell_{\text{max}} = 1000$, and are normalized by $\sqrt{f_{\text{sky}}}$.

For the cross power spectra which have primarily no statistical correlation [i.e., $C_\ell^{n_i n_j}$ ($i \neq j$) and $C_\ell^{\gamma_i n_j}$ ($i < j$)] [59], the signal-to-noise ratios are significantly improved by the magnification effect. For example, the signal-to-noise ratio of $C_\ell^{\gamma_2 n_3}$ increases by a factor of ~ 115 . This is because the magnification effect leads to a non-vanishing correlation between foreground galaxies and the background sources. On the other hand, the improvement of the signal-to-noise ratio is relatively small for the power spectra which have strong statistical correlation even in the absence of the magnification effect [i.e., $C_\ell^{n_i n_j}$ ($i = j$), and $C_\ell^{\gamma_i n_j}$ ($i \geq j$)]. Since the signals of these spectra are primarily very large enough to detect, the results indicate that the size of the constraint on f_{NL} would not be drastically changed even if the magnification effect is properly taken into account in the data analysis. We finally note that, even in the absence of the magnification effect, the signal-to-noise ratios of the shear-galaxy cross correlations [$C_\ell^{\gamma_i n_j}$ ($i \geq j$)] are comparable to that of the galaxy auto correlations [$C_\ell^{n_i n_j}$ ($i = j$)]. This implies that, the parameter f_{NL} would be constrained not only from the galaxy auto correlations, but also from the shear-galaxy cross correlations.

IV. MAGNIFICATION EFFECT ON THE DETECTION OF PRIMORDIAL NON-GAUSSIANITY

In this section, based on the Fisher matrix formalism, we now present the forecast constraint on f_{NL} from photometric surveys, and estimate the size of systematic bias from the incorrect treatment of magnification effect in the theoretical template of angular power spectra. As representative upcoming experiments for wide and/or deep surveys, we consider HSC experiment for wide but narrow, DES for shallow but wide, and LSST for idealistically deep and wide surveys.

A. Fisher matrix formalism

Here, we summarize the Fisher matrix formalism used in the subsequent analysis, and describe the canonical survey setup for photometric galaxy surveys and CMB experiments.

Given the angular power spectra theoretically parametrized by a set of parameters \mathbf{p} , the Fisher matrix for the cosmological parameters is written as (e.g., [60])

$$F_{ij} = \sum_{\ell=2}^{\ell_{\text{max}}} \frac{2\ell+1}{2} f_{\text{sky}} \times \text{Tr} \left(C_\ell^{-1}(\mathbf{p}) \frac{\partial C_\ell}{\partial p_i}(\mathbf{p}) C_\ell^{-1}(\mathbf{p}) \frac{\partial C_\ell}{\partial p_j}(\mathbf{p}) \right) \Big|_{\mathbf{p}=\mathbf{p}^{\text{fid}}}, \quad (22)$$

where the quantity C_ℓ represents the covariance matrix for the angular power spectra, p_i is a cosmological parameter which we want to estimate, and \mathbf{p}^{fid} is the set of fiducial cosmological parameters.

In what follows, using a tomographic technique with the number of redshift bin, N_{bin} , we consider the number density fluctuations $n_1, \dots, n_{N_{\text{bin}}}$ (or $g_1, \dots, g_{N_{\text{bin}}}$ when ignoring the magnification effect), and shear fields, $\gamma_1, \dots, \gamma_{N_{\text{bin}}}$, as observables obtained from the photometric surveys. Since these observables are rather sensitive to the late-time cosmic expansion and/or growth of structure, photometric surveys alone cannot give a tight constraint on all the cosmological parameters. To break the degeneracy between cosmological parameters and improve the constraints, we include the information obtained from the primary CMB anisotropies by Planck [61]. To be specific, we use the temperature (Θ) and (E-mode) polarization (E) data for primary CMB anisotropies. Denoting the noise power spectra by N_ℓ^{XY} , the full covariance matrix, C_ℓ , is written as

$$[C_\ell]_{ij} = C_\ell^{X_i X_j} + N_\ell^{X_i X_j} \delta_{ij}, \quad (23)$$

where X_i and X_j stand for $n_1, \dots, n_{N_{\text{bin}}}$ (or $g_1, \dots, g_{N_{\text{bin}}}$ in the absence of the magnification effect), $\gamma_1, \dots, \gamma_{N_{\text{bin}}}$,

Θ , or E . The amplitude and shape of the noise spectra N_ℓ^{XY} depends on the survey design which will be discussed below.

In the Fisher-matrix analysis, the forecast constraints depend on the properties of a photometric survey, characterized by the sky coverage, f_{sky} , the mean redshift, z_m , and the total number of galaxies per square arcminute, N_g . To show how the constraint on f_{NL} depends on the survey design, we compute the Fisher matrix in the three representative photometric surveys; HSC for a deep survey ($f_{\text{sky}} = 0.05$, $z_m = 1.0$ and $N_g = 35 \text{ arcmin}^{-2}$) and DES ($f_{\text{sky}} = 0.125$, $z_m = 0.5$ and $N_g = 12 \text{ arcmin}^{-2}$) for a wide imaging surveys, and LSST ($f_{\text{sky}} = 0.5$, $z_m = 1.5$ and $N_g = 100 \text{ arcmin}^{-2}$) as an idealistic survey, which is deeper and wider enough than the HSC and DES surveys. In Table I, we summarize the basic parameters of the survey design for three surveys used in the subsequent analysis.

Let us now consider the noise spectra for each data set. In a photometric survey, the main noise source for galaxy counts is the shot noise given by

$$N_\ell^{n_i n_j} = \delta_{ij} \frac{1}{\hat{N}_i}, \quad (24)$$

with the quantity \hat{N}_i being the number density of galaxies per steradians in i -th redshift bin;

$$\hat{N}_i = 3600 \bar{N}_i \left(\frac{180}{\pi} \right)^2 \text{ str}^{-1}. \quad (25)$$

On the other hand, the noise source for cosmic shear measurement mainly comes from the intrinsic ellipticity of galaxies, which is described by

$$N_\ell^{\gamma_i \gamma_j} = \delta_{ij} \frac{\langle \gamma_{\text{int}}^2 \rangle}{\hat{N}_i}. \quad (26)$$

The quantity $\langle \gamma_{\text{int}}^2 \rangle^{1/2}$ is the rms intrinsic ellipticity. We adopt the empirically derived value, $\langle \gamma_{\text{int}}^2 \rangle^{1/2} = 0.3$ [62]. In all surveys, the galaxy samples are divided into three redshift bins, and the ranges of redshift are chosen such that each redshift bin has same number of galaxies, $N_g/3$. The resultant redshift ranges are summarized in Table II for each mean redshift z_m . Note that the noise power spectra of CMB anisotropies, $N_\ell^{\Theta\Theta}$ and N_ℓ^{EE} , are computed according to Eq. (3.3) of Ref.[63], with the experimental specification for Planck [61].

From the Fisher matrix, the $1-\sigma$ (68 %C.L.) constraint on a cosmological parameter, $\sigma(p_i)$, marginalized over other parameters, is given by $\{F_{ii}^{-1}\}^{1/2}$. Number of free parameters in the subsequent Fisher analysis is, in total, 13, i.e., $\Omega_b h^2$, $\Omega_m h^2$, Ω_Λ , n_s , A_s , τ , w , f_{NL} , in addition to the galaxy bias parameters (b_0 and b_z) and slope indices (s_1, s_2, s_3). Note that the number of free parameters is changed to 10 if we incorrectly neglect the magnification effect in the theoretical template of angular power spectra. The fiducial values of the parameters are the same

TABLE I. Survey design for HSC, DES and LSST, i.e., the sky coverage, f_{sky} , the mean redshift, z_m , and the number of galaxies per square arcminute, N_g . In all surveys, the galaxy samples are divided into three redshift bin, and the ranges of redshift are chosen such that the each redshift bin has same number of galaxies, $N_g/3$. The resultant redshift ranges are summarized in Table II for each mean redshift z_m .

Survey	f_{sky}	z_m	$N_g [\text{arcmin}^{-2}]$
HSC [31]	0.05 (2000deg ²)	1.0	35
DES [32]	0.125 (5000deg ²)	0.5	12
LSST [33]	0.5 (20000deg ²)	1.5	100

TABLE II. The relation between mean redshift, z_m , and the redshift ranges of i -th bin computed in the case with $N_{\text{bin}} = 3$. Using Eq.(13), the redshift ranges are determined such that each redshift bin has same number of galaxies.

z_m	redshift ranges		
0.5	$z < 0.369$	$0.369 < z < 0.569$	$0.569 < z$
1.0	$z < 0.739$	$0.739 < z < 1.14$	$1.14 < z$
1.5	$z < 1.11$	$1.11 < z < 1.72$	$1.72 < z$
2.0	$z < 1.48$	$1.48 < z < 2.29$	$2.29 < z$

as those in Sec.III, and we assume that the photo- z error and redshift distribution of galaxies are given in Eq.(17) and Eq.(16), respectively.

Using the Fisher matrix formalism, we also evaluate the systematic bias in the best-fit value of cosmological parameters, Δp_i , arising from the incorrect treatment of the magnification effect in the theoretical template. Assuming the Gaussian likelihood function, the bias of the best-fit value, Δp_i , can be estimated from [64]

$$\Delta p_i = \frac{1}{2} \sum_{i,j} \tilde{F}_{ij} \frac{2\ell+1}{2} f_{\text{sky}} \times \text{Tr} \left(\tilde{C}^{-1}(\mathbf{p}) \frac{\partial \tilde{\mathbf{C}}}{\partial p_i}(\mathbf{p}) \tilde{C}^{-1}(\mathbf{p}) (\mathbf{C}(\mathbf{p}) - \tilde{\mathbf{C}}(\mathbf{p})) \right) \Big|_{\mathbf{p}=\mathbf{p}^{\text{fid}}}, \quad (27)$$

where the covariance matrices \mathbf{C} and $\tilde{\mathbf{C}}$ are computed with and without the magnification effect in the power spectra, respectively. The Fisher matrix \tilde{F}_{ij} is computed by ignoring the magnification in angular power spectra.

B. Results

1. Estimation of primordial non-Gaussianity for representative surveys

Here we present forecast results for the constraint on primordial non-Gaussianity, especially focusing on the following cases:

- $+n$: using galaxy counts alone *taking into account* the magnification effect in the theoretical template ($C_\ell^{n_i n_j}$),

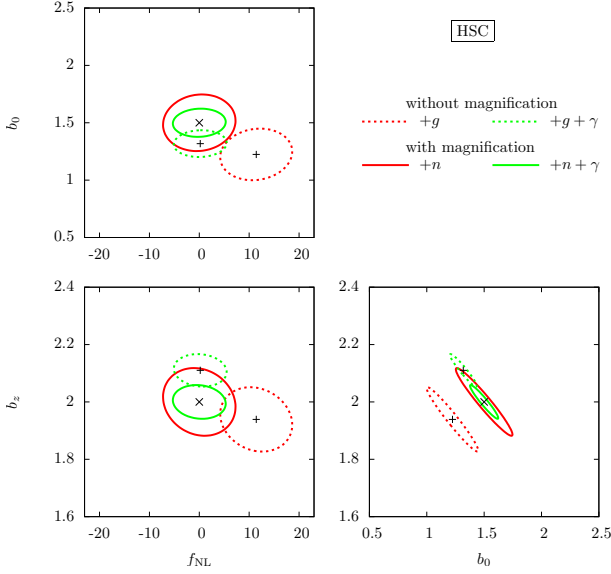


FIG. 4. The $1\text{-}\sigma$ error contours on b_0 - f_{NL} (top left), b_z - f_{NL} (bottom left) and b_z - b_0 (bottom right) planes for HSC. In each panel, we show the constraints in the case with (solid) and without (dashed) the magnification effect in theoretical template. In each case, we show the results obtained from galaxy number counts alone, and further including cosmic shear of galaxies. Note that CMB prior information from Planck is included in all cases. Information from the primary CMB is summed up to $\ell = 3000$, and other signals are included up to $\ell_{\text{max}} = 1000$. We also note that the fiducial values of the galaxy bias parameters and slope indices are chosen as $b_0 = 1.5$, $b_z = 2.0$, $s_1 = 0.5$, $s_2 = 1.0$ and $s_3 = 1.5$.

TABLE III. The $1\text{-}\sigma$ constraints, $\sigma(f_{\text{NL}})$, and the systematic bias, Δf_{NL} , on the primordial non-Gaussianity, in the case with/without the magnification effect in theoretical template. In each case, we show the resultant constraints obtained from galaxy number counts alone, and further including cosmic shear of galaxies. CMB prior information from Planck is included in all cases. We set the maximum multipole as $\ell_{\text{max}} = 1000$, but the primary CMB power spectra is used up to $\ell = 3000$ in the Fisher matrix.

	HSC		DES		LSST	
	$\sigma(f_{\text{NL}})$	Δf_{NL}	$\sigma(f_{\text{NL}})$	Δf_{NL}	$\sigma(f_{\text{NL}})$	Δf_{NL}
+n	4.8	-	9.8	-	0.86	-
+g	4.7	11	9.7	21	0.86	7.1
+n + γ	3.5	-	8.2	-	0.49	-
+g + γ	3.5	0.19	8.2	1.7	0.49	-0.76

- +g: using galaxy counts alone *neglecting* the magnification effect in the theoretical template ($C_\ell^{g_i g_j}$),
- +n + γ : combining galaxy counts, cosmic shear, and their cross-correlations *taking into account* the effect of magnification ($C_\ell^{n_i n_j}$, $C_\ell^{\gamma_i n_j}$, $C_\ell^{\gamma_i \gamma_j}$),
- +g + γ : combining galaxy counts, cosmic shear,

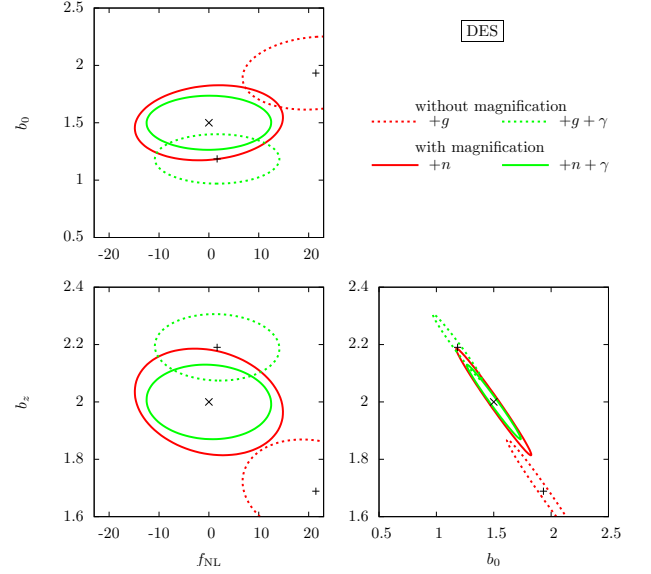


FIG. 5. Same as Fig.4 but for DES.

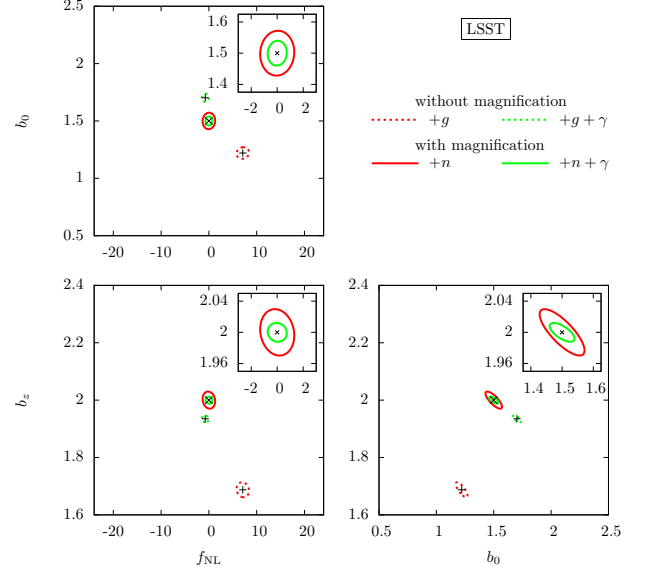


FIG. 6. Same as Fig.4 but for LSST. The inset shows the zoomed error contours around the fiducial values.

and their cross-correlations *neglecting* the effect of magnification, ($C_\ell^{g_i g_j}$, $C_\ell^{\gamma_i g_j}$, $C_\ell^{\gamma_i \gamma_j}$).

Note that, in all cases, we add the primary CMB information (i.e., $C_\ell^{\Theta\Theta}$, $C_\ell^{\Theta E}$ and C_ℓ^{EE}) in the Fisher matrix. The primary CMB power spectra are used to estimate the cosmological parameters up to $\ell = 3000$. In Table III, we show the forecast results of $1\text{-}\sigma$ constraints on f_{NL} for three representative surveys. Also, in Figs.4-6, two-dimensional contours of $1\text{-}\sigma$ error on b_z - f_{NL} , b_0 - f_{NL} and b_0 - b_z planes are plotted in the cases of HSC, DES and LSST taking into account or neglecting the magnifi-

cation effect.

Let us focus on the results from the galaxy counts alone, i.e., $+n$ and $+g$ (see red solid and dashed lines in Figs.4-6). Naively, the statistical error on f_{NL} is expected to be large if we properly take account of the magnification effect, because we need to specify the slope indices observationally and the number of parameters to be determined increases. As shown in Figs.4-6, however, the statistical error on f_{NL} does not change so much in all cases, and the fractional change is around a sub-percent level (see Table.III). These figures also show that, as mentioned in Sec.III, the degeneracy between f_{NL} and the galaxy bias (b_0 and b_z) is weak (the correlation coefficient is ~ 0.1). On the other hand, the systematic bias on f_{NL} arising from the incorrect treatment of the magnification effect is significant. As shown in Table. III, the systematic bias is apparently very large for DES. Taking the ratio of the systematic bias to the statistical error, however, the largest value is obtained from the LSST case amongst three surveys. That is, the systematic bias is rather serious for LSST than for HSC or DES.

Next discuss the importance of cosmic shear information, i.e., $+n + \gamma$ and $+g + \gamma$ (see green solid and dashed lines in Figs. 4-6). Compared to the cases with galaxy counts alone, the addition of cosmic shear data would not only improve the statistical error, but also reduce the systematic bias on f_{NL} , irrespective of the treatment of the magnification effect. These results basically come from the non-vanishing shear-galaxy correlations, which also carry the information on f_{NL} through the scale-dependent galaxy bias, as shown in Fig. 1. Table. III shows that compared to the results with galaxy counts alone, the improvement of the constraint is by a factor of ~ 2 for LSST and of $\sim 1.3 - 1.5$ for HSC and DES. The size of systematic bias on f_{NL} is now well within the $1-\sigma$ statistical error for HST and DES, but it is still non-negligible for LSST.

2. Dependence on maximum multipole ℓ_{max} , mean redshift z_m , number of redshift bin N_{bin} , and slope s_i

To elucidate the results in Sec.IV B 1 in more details, we here consider the dependence of the systematic bias and statistical error on the various parameters, especially focusing on the LSST-like survey. Fig. 7 shows the systematic bias Δf_{NL} using the tomographic technique with $N_{\text{bin}} = 3$, plotted against the maximum multipole used in the parameter estimation, ℓ_{max} . In each panel, the results obtained from a different survey depth are presented; $z_m = 0.5, 1.0, 1.5$ and 2.0 (in each case, redshift ranges of each redshift bin are summarized in Table. II). To infer the significance of the systematic bias, we also plot the $1-\sigma$ constraint on f_{NL} , $\sigma(f_{\text{NL}})$, taking a proper account of the magnification effect (shaded region). Fig. 8 also shows the same results as in Fig. 7, but, this time, we do not use the tomographic technique (i.e., $N_{\text{bin}} = 1$), and the slope index is simply set to

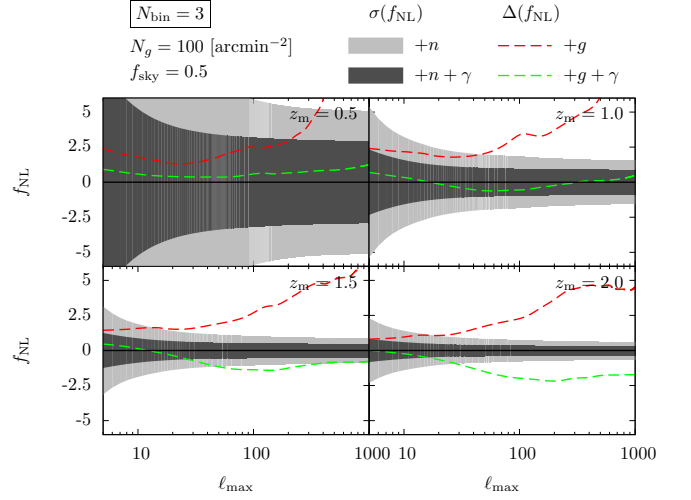


FIG. 7. The systematic bias on f_{NL} as a function of ℓ_{max} for $+g$ (red) and $+g + \gamma$ (green). The shaded regions denote the $1-\sigma$ constraint on f_{NL} for $+n$ (thin) and $+n + \gamma$ (thick). Each panel show the case with $z_m = 0.5, 1.0, 1.5$ and 2.0 . The galaxy subsamples are divided into three redshift bins ($N_{\text{bin}} = 3$). We assume $N_g = 100 \text{ arcmin}^{-2}$ and $f_{\text{sky}} = 0.5$.

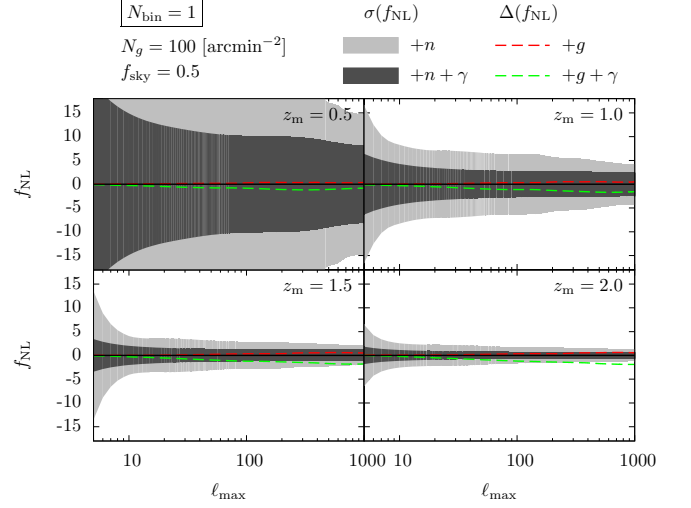


FIG. 8. Same as Fig.7 but for $N_{\text{bin}} = 1$. In this case, we choose the slope as $s_1 = 1.0$. Note that the range of y -axis is three times larger than that in Fig.7.

$s_1 = 1.0$. Note that the systematic bias does not depend on f_{sky} , while the $1-\sigma$ constraint is proportional to $\sqrt{f_{\text{sky}}}$. Also, for a sufficiently large number density with $N_g \gtrsim 10 \text{ arcmin}^{-2}$, the results are almost insensitive to the choice of N_g . Hence, the noise spectra are computed with fixed values of $f_{\text{sky}} = 0.5$ and $N_g = 100 \text{ arcmin}^{-2}$.

Let us consider the results using the galaxy counts alone with $N_{\text{bin}} = 3$ (see Fig.7). As increasing z_m , the statistical error on f_{NL} (the thin shaded region) becomes rather improved, and the systematic bias (the red dashed

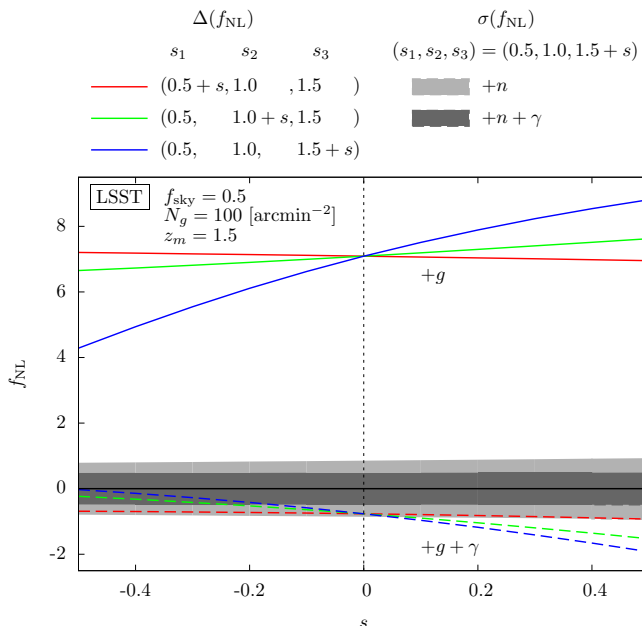


FIG. 9. Dependence of the systematic bias and $1\text{-}\sigma$ constraint on the slope parameter. We vary only the one slope parameter (s_1 , s_2 or s_3) and parametrized by a parameter s as $s_1 = 0.5 + s$, $s_2 = 1.0 + s$, or $s_3 = 1.5 + s$. The parameter s is varied from -0.5 to 0.5 . The red, green and blue lines show the systematic bias with varying s_1 , s_2 and s_3 , respectively. The gray and black shaded regions represent the $1\text{-}\sigma$ constraint in the case of $+g$ and $+g + \gamma$, respectively, with varying the slope parameter in third redshift bin, s_3 . We assume LSST to calculate the noise spectrum.

lines) is somehow reduced if we choose a large maximum multipole. However, for a deep survey with $z_m \gtrsim 1.5$ (bottom panels), the systematic bias is still non-negligible compared to the statistical error on f_{NL} . This is true even if we include the cosmic shear data (the green dashed lines).

Next discuss the importance of tomographic technique. Comparison between Figs. 8 and 7 implies that the tomographic technique is quite helpful to reduce the statistical error of f_{NL} . Typically, with $N_{\text{bin}} = 3$, the error would be reduced by a factor of $\sim 2 - 3$. This is partly because the amplitude of the large-scale galaxy clustering sensitively depends on the redshift in the presence of the scale-dependent galaxy bias (see Eq. (3) and Fig. 2). Presumably, this may also break the degeneracy between f_{NL} and slope indices. Note, however, that the tomographic technique do not help to reduce the systematic bias, but rather it increases the size of bias. In this respect, a proper account of the magnification effect in the theoretical template is crucial in a LSST-like survey.

So far, the fiducial values of the slope indices have been held fixed. In order to clarify the influence of the slope indices, keeping the number of redshift bins $N_{\text{bin}} = 3$, we allow to vary one of the three slope indices around the fiducial values, and estimate the systematic bias and sta-

tistical error on f_{NL} . Fig. 9 shows the results in the case of the LSST survey. Here, the results are plotted against the shift of the slope index, s , defined by $s_i = s_{i,\text{fid}} + s$. The lines with different color indicate the systematic bias of f_{NL} obtained by varying the different slope index. Note that the statistical errors depicted as shaded regions are evaluated specifically in the case varying the slope s_3 .

Fig. 9 indicates that the systematic bias of f_{NL} is insensitive to the variation of slope index in lower redshift bin, but rather sensitive to it at higher redshift bin. This result is quite reasonable because the magnification effect at high- z bin is significant compared to low- z bin (see Fig 2). On the other hand, the statistical error on f_{NL} is insensitive to the variation of slope index, as it is expected from Sec. III B. In this respect, depending on the value of slope indices at high redshifts, the magnification effect on constraining primordial non-Gaussianity may become even more serious, and again, should be properly taken into account in the theoretical template.

V. SUMMARY

In this paper, we studied the impact of magnification effect on the detection of f_{NL} from photometric survey. As representative upcoming photometric surveys, we considered HSC for deep, and DES for wide, and LSST for an idealistically deep and wide survey. From the Fisher matrix analysis, we showed that, an incorrect treatment of the magnification effect on the theoretical template of angular power spectra leads to the systematic bias in the best-fit value of f_{NL} . Especially, using galaxy counts alone, the size of systematic bias is significant for all three surveys (HSC, DES and LSST), and true values of f_{NL} would typically go outside the $3\text{-}\sigma$ error of the biased confidence region. However, we found that additional information from the cosmic shear observations helps not only to improve the constraint, but also to reduce the systematic bias on f_{NL} . As a result, the systematic bias can become negligible for HSC and DES surveys, compared to their expected errors on f_{NL} . A proper account of the magnification effect does not increase the statistical error on f_{NL} ($\lesssim 1\%$). Nevertheless, for LSST, a relative significance of the systematic bias still remains and the magnification effect should be correctly taken into account in the theoretical treatment.

We further explored the various cases by changing parameters characterizing the survey properties, and showed that the tomographic technique using photometric redshift information leads to a significant improvement on the statistical error on f_{NL} , but it does not help to reduce the systematic bias. In any case, high- z observations are indispensable for tightly constraining primordial non-Gaussianity, but the influence of the magnification effect would be inevitable. This is particularly true for deep imaging surveys like LSST ($z_m \gtrsim 1.5$). A proper account of the magnification effect in the theoretical template is thus quite essential for an unbiased estimate of

primordial non-Gaussianity.

ACKNOWLEDGMENTS

We would like to thank Emiliano Sefusatti and Fabian Schmidt for useful comments and discussions about the size bias. We are also grateful to Eiichiro Komatsu and Toshifumi Futamase for helpful discussions. TO and AT

are supported in part by a Grants-in-Aid for Scientific Research from the Japan Society for the Promotion of Science (JSPS) (No. 22-2879 for TO and No. 21740168 for AT). This work was supported in part by Grant-in-Aid for Scientific Research on Priority Areas No. 467 "Probing the Dark Energy through an Extremely Wide and Deep Survey with Subaru Telescope", the GCOE Program "Weaving Science Web beyond Particle-matter Hierarchy" at Tohoku University, and JSPS Core-to-Core Program "International Research Network for Dark Energy".

-
- [1] T. J. Allen, B. Grinstein, and M. B. Wise, *Non-gaussian density perturbations in inflationary cosmologies*, *Physics Letters B* **197** (oct, 1987) 66–70.
 - [2] D. S. Salopek and J. R. Bond, *Nonlinear evolution of long-wavelength metric fluctuations in inflationary models*, *Phys. Rev.* **42** (dec, 1990) 3936–3962.
 - [3] T. Falk, R. Rangarajan, and M. Srednicki, *Dependence of density perturbations on the coupling constant in a simple model of inflation*, *Phys. Rev.* **D46** (1992) 4232–4234, [[astro-ph/9208002](#)].
 - [4] A. Gangui, F. Lucchin, S. Matarrese, and S. Mollerach, *The Three point correlation function of the cosmic microwave background in inflationary models*, *Astrophys. J.* **430** (1994) 447–457, [[astro-ph/9312033](#)].
 - [5] J. M. Maldacena, *Non-Gaussian features of primordial fluctuations in single field inflationary models*, *JHEP* **05** (2003) 013, [[astro-ph/0210603](#)].
 - [6] V. Acquaviva, N. Bartolo, S. Matarrese, and A. Riotto, *Second-order cosmological perturbations from inflation*, *Nucl. Phys.* **B667** (2003) 119–148, [[astro-ph/0209156](#)].
 - [7] N. Bartolo, E. Komatsu, S. Matarrese, and A. Riotto, *Non-Gaussianity from inflation: Theory and observations*, *Phys. Rept.* **402** (2004) 103–266, [[astro-ph/0406398](#)].
 - [8] E. Komatsu and D. N. Spergel, *Acoustic signatures in the primary microwave background bispectrum*, *Phys. Rev.* **D63** (2001) 063002, [[astro-ph/0005036](#)].
 - [9] D. Babich and M. Zaldarriaga, *Primordial Bispectrum Information from CMB Polarization*, *Phys. Rev.* **D70** (2004) 083005, [[astro-ph/0408455](#)].
 - [10] E. Sefusatti and E. Komatsu, *The bispectrum of galaxies from high-redshift galaxy surveys: Primordial non-Gaussianity and non-linear galaxy bias*, *Phys. Rev.* **D76** (2007) 083004, [[arXiv:0705.0343](#)].
 - [11] M. Liguori *et al.*, *Temperature and Polarization CMB Maps from Primordial non-Gaussianities of the Local Type*, *Phys. Rev.* **D76** (2007) 105016, [[arXiv:0708.3786](#)].
 - [12] E. Komatsu *et al.*, *Non-Gaussianity as a Probe of the Physics of the Primordial Universe and the Astrophysics of the Low Redshift Universe*, [arXiv:0902.4759](#).
 - [13] D. Jeong and E. Komatsu, *Primordial non-Gaussianity, scale-dependent bias, and the bispectrum of galaxies*, *Astrophys. J.* **703** (2009) 1230–1248, [[arXiv:0904.0497](#)].
 - [14] N. Dalal, O. Dore, D. Huterer, and A. Shirokov, *The imprints of primordial non-gaussianities on large-scale structure: scale dependent bias and abundance of virialized objects*, *Phys. Rev.* **D77** (2008) 123514, [[arXiv:0710.4560](#)].
 - [15] V. Desjacques, U. Seljak, and I. Iliev, *Scale-dependent bias induced by local non-Gaussianity: A comparison to N-body simulations*, [arXiv:0811.2748](#).
 - [16] L. Verde and S. Matarrese, *Detectability of the effect of Inflationary non-Gaussianity on halo bias*, *Astrophys. J.* **706** (2009) L91–L95, [[arXiv:0909.3224](#)].
 - [17] T. Nishimichi, A. Taruya, K. Koyama, and C. Sabiu, *Scale Dependence of Halo Bispectrum from Non-Gaussian Initial Conditions in Cosmological N-body Simulations*, *JCAP* **1007** (2010) 002, [[arXiv:0911.4768](#)].
 - [18] A. Taruya, K. Koyama, and T. Matsubara, *Signature of Primordial Non-Gaussianity on Matter Power Spectrum*, *Phys. Rev.* **D78** (2008) 123534, [[arXiv:0808.4085](#)].
 - [19] A. Pillepich, C. Porciani, and O. Hahn, *Universal halo mass function and scale-dependent bias from N-body simulations with non-Gaussian initial conditions*, [arXiv:0811.4176](#).
 - [20] T. Giannantonio and C. Porciani, *Structure formation from non-Gaussian initial conditions: multivariate biasing, statistics, and comparison with N-body simulations*, *Phys. Rev.* **D81** (2010) 063530, [[arXiv:0911.0017](#)].
 - [21] M. Grossi *et al.*, *Large-scale non-Gaussian mass function and halo bias: tests on N-body simulations*, *Mon. Not. Roy. Astron. Soc.* **398** (2009) 321–332, [[arXiv:0902.2013](#)].
 - [22] S. Matarrese and L. Verde, *The effect of primordial non-Gaussianity on halo bias*, *Astrophys. J.* **677** (2008) L77–L80, [[arXiv:0801.4826](#)].
 - [23] F. Schmidt and M. Kamionkowski, *Halo Clustering with Non-Local Non-Gaussianity*, *Phys. Rev.* **D82** (2010) 103002, [[arXiv:1008.0638](#)].
 - [24] V. Desjacques and U. Seljak, *Primordial non-Gaussianity in the large scale structure of the Universe*, [arXiv:1006.4763](#).
 - [25] V. Desjacques and U. Seljak, *Primordial non-Gaussianity from the large scale structure*, *Class. Quant. Grav.* **27** (2010) 124011, [[arXiv:1003.5020](#)].
 - [26] J. S. Bullock and J. R. Primack, *Comments on non-Gaussian density perturbations and the production of primordial black holes*, [astro-ph/9806301](#).
 - [27] L. Verde, L.-M. Wang, A. Heavens, and

- M. Kamionkowski, *Large-scale structure, the cosmic microwave background, and primordial non-gaussianity*, *Mon. Not. Roy. Astron. Soc.* **313** (2000) L141–L147, [astro-ph/9906301].
- [28] A. Slosar, C. Hirata, U. Seljak, S. Ho, and N. Padmanabhan, *Constraints on local primordial non-Gaussianity from large scale structure*, *JCAP* **0808** (2008) 031, [arXiv:0805.3580].
- [29] N. Afshordi and A. J. Tolley, *Primordial non-gaussianity, statistics of collapsed objects, and the Integrated Sachs-Wolfe effect*, *Phys. Rev.* **D78** (2008) 123507, [arXiv:0806.1046].
- [30] J.-Q. Xia *et al.*, *Constraining Primordial Non-Gaussianity with High-Redshift Probes*, *JCAP* **1008** (2010) 013, [arXiv:1007.1969].
- [31] HSC Collaboration, *Hyper Suprime-Cam Design Review*. 2009.
- [32] T. Abbott *et al.*, *The dark energy survey*. 2005.
- [33] LSST Science Collaboration, *LSST Science Book, Version 2.0*. 2009.
- [34] SDSS Collaboration, R. Scranton *et al.*, *Detection of Cosmic Magnification with the Sloan Digital Sky Survey*, *Astrophys. J.* **633** (2005) 589–602, [astro-ph/0504510].
- [35] H. Hildebrandt, L. van Waerbeke, and T. Erben, *CARS: The CFHTLS-Archive-Research Survey III. First detection of cosmic magnification in samples of normal high- z galaxies*, arXiv:0906.1580.
- [36] L. Wang *et al.*, *HerMES: detection of cosmic magnification of sub-mm galaxies using angular cross-correlation*, arXiv:1101.4796.
- [37] C. Carbone, L. Verde, and S. Matarrese, *Non-Gaussian halo bias and future galaxy surveys*, *Astrophys. J.* **684** (2008) L1–L4, [arXiv:0806.1950].
- [38] C. Carbone, O. Mena, and L. Verde, *Cosmological Parameters Degeneracies and Non-Gaussian Halo Bias*, *JCAP* **1007** (2010) 020, [arXiv:1003.0456].
- [39] Y. Takeuchi, K. Ichiki, and T. Matsubara, *Constraints on primordial non-Gaussianity from Galaxy-CMB lensing cross-correlation*, *Phys. Rev.* **D82** (2010) 023517, [arXiv:1005.3492].
- [40] A. Lewis, A. Challinor, and A. Lasenby, *Efficient Computation of CMB anisotropies in closed FRW models*, *Astrophys. J.* **538** (2000) 473–476, [astro-ph/9911177].
- [41] E. Komatsu *et al.*, *Seven-Year Wilkinson Microwave Anisotropy Probe (WMAP) Observations: Cosmological Interpretation*, arXiv:1001.4538.
- [42] The Virgo Consortium Collaboration, R. E. Smith *et al.*, *Stable clustering, the halo model and nonlinear cosmological power spectra*, *Mon. Not. Roy. Astron. Soc.* **341** (2003) 1311, [astro-ph/0207664].
- [43] B. A. Reid, L. Verde, K. Dolag, S. Matarrese, and L. Moscardini, *Non-Gaussian halo assembly bias*, *JCAP* **1007** (2010) 013, [arXiv:1004.1637].
- [44] R. Moessner, B. Jain, and J. V. Villumsen, *The Effect of Weak Lensing on the Angular Correlation Function of Faint Galaxies*, astro-ph/9708271.
- [45] M. Bartelmann and P. Schneider, *Weak Gravitational Lensing*, *Phys. Rept.* **340** (2001) 291–472, [astro-ph/9912508].
- [46] T. Matsubara, *The Gravitational Lensing in Redshift-space Correlation Functions of Galaxies and Quasars*, astro-ph/0004392.
- [47] F. Schmidt, E. Rozo, S. Dodelson, L. Hui, and E. Sheldon, *Size Bias in Galaxy Surveys*, *Phys. Rev. Lett.* **103** (2009) 051301, [arXiv:0904.4702].
- [48] F. Schmidt, E. Rozo, S. Dodelson, L. Hui, and E. Sheldon, *Lensing Bias in Cosmic Shear*, *Astrophys. J.* **702** (2009) 593–602, [arXiv:0904.4703].
- [49] W. Hu, *Weak lensing of the CMB: A harmonic approach*, *Phys. Rev.* **D62** (2000) 043007, [astro-ph/0001303].
- [50] M. LoVerde, L. Hui, and E. Gaztanaga, *Magnification-Temperature Correlation: the Dark Side of ISW Measurements*, *Phys. Rev.* **D75** (2007) 043519, [astro-ph/0611539].
- [51] R. Ziour and L. Hui, *Magnification Bias Corrections to Galaxy-Lensing Cross-Correlations*, *Phys. Rev.* **D78** (2008) 123517, [arXiv:0809.3101].
- [52] L. Hui, E. Gaztanaga, and M. LoVerde, *Anisotropic Magnification Distortion of the 3D Galaxy Correlation: I. Real Space*, *Phys. Rev.* **D76** (2007) 103502, [arXiv:0706.1071].
- [53] A. Amara and A. Refregier, *Optimal Surveys for Weak Lensing Tomography*, *Mon. Not. Roy. Astron. Soc.* **381** (2007) 1018–1026, [astro-ph/0610127].
- [54] W. Hu and R. Scranton, *Measuring Dark Energy Clustering with CMB-Galaxy Correlations*, *Phys. Rev.* **D70** (2004) 123002, [astro-ph/0408456].
- [55] J. N. Fry, *The Evolution of Bias*, *Astrophys. J.* **461** (1996) L65–L67.
- [56] M. Tegmark and P. J. E. Peebles, *The Time evolution of bias*, astro-ph/9804067.
- [57] K. Yamamoto, B. A. Bassett, R. C. Nichol, and Y. Suto, *Searching for modified gravity with baryon oscillations: From SDSS to WFMOS*, *Phys. Rev.* **D74** (2006) 063525, [astro-ph/0605278].
- [58] K. Yamamoto, D. Parkinson, T. Hamana, R. C. Nichol, and Y. Suto, *Optimizing future imaging survey of galaxies to confront dark energy and modified gravity models*, *Phys. Rev.* **D76** (2007) 023504, [arXiv:0704.2949].
- [59] Due to the photo- z error, however, there appears statistical correlation even in the absence of magnification effect, although the signal is very weak.
- [60] M. Tegmark, A. Taylor, and A. Heavens, *Karhunen-Loeve eigenvalue problems in cosmology: how should we tackle large data sets?*, *Astrophys. J.* **480** (1997) 22, [astro-ph/9603021].
- [61] Planck Collaboration, *Planck: The scientific programme*. 2006.
- [62] G. M. Bernstein and M. Jarvis, *Shapes and Shears, Stars and Smears: Optimal Measurements for Weak Lensing*, *Astron. J.* **123** (2002) 583–618, [astro-ph/0107431].
- [63] T. Namikawa, S. Saito, and A. Taruya, *Probing dark energy and neutrino mass from upcoming lensing experiments of CMB and galaxies*, *JCAP* **1012** (2010) 027, [arXiv:1009.3204].
- [64] B. Joachimi and P. Schneider, *The removal of shear-ellipticity correlations from the cosmic shear signal: Influence of photometric redshift errors on the nulling technique*, arXiv:0905.0393.